

On the energy distribution of relativistic electrons in the young supernova remnant G1.9+0.3

Rui-zhi Yang¹, Xiao-na Sun¹, and Felix Aharonian^{1,2,3,4}

¹ Max-Planck-Institut für Kernphysik, P.O. Box 103980, 69029 Heidelberg, Germany.

² Dublin Institute for Advanced Studies, 31 Fitzwilliam Place, Dublin 2, Ireland.

³ Gran Sasso Science Institute, 7 viale Francesco Crispi, 67100 L'Aquila (AQ), Italy

⁴ MEPHI, Kashirskoe shosse 31, 115409 Moscow, Russia

Received: / Accepted:

ABSTRACT

The broad-band X-ray observations of the youngest known galactic supernova remnant, G1.9+0.3, provide unique information about the particle acceleration at the early stages of evolution of supernova remnants. Based on the publicly available X-ray data obtained with the Chandra and NuSTAR satellites over two decades in energy, we derived the energy distribution of relativistic electrons under the assumption that detected X-rays are of entirely synchrotron origin. The acceleration of electrons was found to be an order of magnitude slower than the maximum rate provided by the shock acceleration in the nominal Bohm diffusion regime. We discuss the implications of this result in the context of contribution of SNRs to the Galactic Cosmic Rays at PeV energies.

Key words. X-rays: individuals: SNR G1.9+0.3; Acceleration of particles; cosmic rays

1. Introduction

Supernova Remnants (SNRs) are believed to be the sites where the bulk of Galactic Cosmic Rays (CRs) are accelerated up to PeV energies ($1 \text{ PeV} = 10^{15} \text{ eV}$) (see, e.g., Hillas 2013; Blasi 2013). In recent years, significant progress has been achieved in a few directions of exploring the CR acceleration in SNRs, in particular using the γ -ray observations in the MeV/GeV and TeV energy bands (see, e.g., Aharonian 2013). In particular, the detection of the so-called π^0 -decay bump in the spectra of several mid-age SNRs, is considered as a substantial evidence of acceleration of protons and nuclei in SNRs. Moreover, the detection of more than ten young (a few thousand years old or younger) SNRs in TeV γ -rays highlights these objects as efficient particle accelerators, although the very origin of γ -rays (leptonic or hadronic?) is not yet firmly established. More disappointingly, so far all TeV emitting SNRs do not show energy spectra which would continue as a hard power-law beyond 10 TeV. For a hadronic origin of detected γ -rays, the "early" cutoffs in the energy spectra of γ -rays around or below 10 TeV imply a lack of protons inside the shells of SNRs with energies significantly larger than 100 TeV, and, consequently, SNRs do not operate as PeVatrons. However, there are two possibilities would allow us to avoid such a dramatic, for the current paradigm of Galactic CRs, conclusion:

(i) The detected TeV gamma-rays are of leptonic (Inverse Compton) origin. Of course, alongside with the relativistic electrons, protons and nuclei can (should) be accelerated as well, but we do not see the related γ -radiation because of their ineffective interactions caused by the low density of ambient gas;

(ii) SNRs do accelerate protons to PeV energies, however it occurs at early stages of evolution of SNRs when the shock speeds exceed 10,000 km/s; we do not see the corresponding radiation well above 10 TeV because the PeV protons already have left the remnant.

Both these scenarios significantly limit the potential of gamma-ray observations for the search for CR PeVatrons. Fortunately, there is another radiation component which contains an independent and complementary information about these extreme accelerators. It is related to the synchrotron radiation of accelerated electrons, namely to the shape of the energy spectrum of radiation in the cutoff region which can serve as a distinct signature of the acceleration mechanism and its efficiency. In the shock acceleration scheme, the maximum energy of accelerated particles, $E_0 \propto B v_{\text{sh}}^2$. Therefore, the epoch of first several hundred years of evolution of a SNR, when the shock speed v_{sh} exceeds 10,000 km/s and the magnetic field is large, $B \gg 10 \mu\text{G}$, could be an adequate stage for operation of a SNR as a PeVatron, provided, of course, that the shock acceleration proceeds close to the Bohm diffusion limit (see, e.g., Malkov & Drury 2001). Remarkably, in this regime, the cutoff energy in the synchrotron radiation of the shock-accelerated electrons is determined by a single parameter, v_{sh}^2 (Aharonian & Atoyan 1999; Zirakashvili & Aharonian 2007). Therefore, for the known shock speed, the position of the cutoff contains an unambiguous information about the acceleration efficiency. For $v_{\text{sh}} \approx 10,000 \text{ km/s}$, the synchrotron cutoff in the spectral energy distribution (SED) is expected around 10 keV. Thus, the study of synchrotron radiation in the hard X-ray band can shed light on the acceleration efficiency of electrons, and, consequently, provide an answer whether these objects can operate as CR PeVatrons, given that in the shock acceleration scheme the acceleration of electrons and protons is expected to be identical. In this regard, G1.9+0.3, the youngest known SNR in our Galaxy (Reynolds et al. 2008; Green et al. 2008), is a perfect object to explore this unique tool.

The X-ray observations with the Chandra and NuSTAR satellites (Reynolds et al. 2009; Zoglauer et al. 2015) cover a rather broad energy interval which is crucial for the study of the spec-

tral shape of synchrotron radiation in the cutoff region. Such a study has been conducted by the team of the NuSTAR collaboration (Zoglauer et al. 2015). However, some conclusions and statements of that paper seem to us rather confusing and, to a certain extent, misleading.

In this paper we present the results of our own analysis of the NuSTAR and Chandra data with an emphasis on the study of the SED of X-radiation over two decades, from 0.3 keV to 30 keV. Using the synchrotron spectrum and the Markov Chain Monte Carlo (MCMC) technique, we derive the energy distribution of electrons responsible for X-rays, and discuss the astrophysical implications of the obtained results.

2. X-ray observations

The recent hard X-ray observations of G1.9+0.3 by the NuSTAR satellite are unique for understanding of the acceleration and radiation processes of ultrarelativistic electrons in SNRs at the early stages of their evolution. The detailed study of the NuSTAR data, combined with the Chandra observations at lower energies, have been comprehensively analysed by Zoglauer et al. (2015). In particular, it was found that the source can be resolved into two bright limbs with similar spectral features. The combined Chandra and NuSTAR data sets have been claimed to be best described by the so-called *srcut* model (Reynolds 2008) or by the power-law function with an exponential cutoff. The characteristic cutoff energies in these two fits have been found around 3 keV and 15 keV, respectively (Zoglauer et al. 2015).

To further investigate the features of the X-ray spectrum in the cutoff region we performed an independent study based on the publicly available Chandra and NuSTAR X-ray data. For NuSTAR, we used the set of three observations with ID 40001015003, 40001015005, 40001015007, including both the focal plane A (FPMA) and B (FPMB) modules. The data have been analysed using the HEASoft version 6.16, which includes NuSTARDAS, the NuSTAR Data Analysis Software package (the version 1.7.1 with the NuSTAR CALDB version 20150123). For the Chandra data, we used the ACIS observations with ID 12691, 12692 and 12694. The Chandra data reduction was performed by using the version 4.7 of the CIAO (Chandra Interactive Analysis of Observations) package.

In Fig.1 we show the X-ray sky map above 3 keV based on the NuSTAR 40001015007 data set. In order to gain from the maximum possible statistics, for the spectral analysis we have chosen the entire remnant. The background regions were selected in a way to minimise the contamination caused by the PSF wings as well as from the stray light. The excess in the south of the FPMA image is the stray light from X-rays that hit the detector without impinging on the optics (Wik et al. 2014). We use the same source regions for Chandra observations. The results of our study of the the spatial distribution of X-rays appeared quite similar the one reported by (Zoglauer et al. 2015). Therefore, in this paper we do not discuss the morphology of the source but focus on the study of spectral features of radiation.

The spectral shape of synchrotron radiation in the cutoff region is sensitive to the spectrum of highest energy electrons which, in its turn, depends on the electron acceleration and energy loss rates. To explore a broad class of spectra, we describe the spectrum of X-rays in the following general form:

$$\frac{dN}{d\epsilon} = AE^{-\Gamma} \exp[-(\epsilon/\epsilon_0)^\beta]. \quad (1)$$

The change of the index β in the second (exponential) term allows a broad range of spectral behaviour in the cutoff region.

For example, $\beta = 0$ implies a pure power-law distribution, while $\beta = 1$ corresponds to a power-law with a simple exponential cutoff.

In the fitting procedure, in addition to the three parameters ϵ_0 , Γ and β , one should introduce one more parameter, the column density N_H , which takes into account the energy-dependent absorption of X-rays. We fix this parameter to the value found by Zoglauer et al. (2015) from the fit of data by their *srcut* spectral model. Strictly speaking, the best fit value of the column density should be different for different spectral model. To check the impact of different spectral models on the column density, we adopted different functions leaving the column density as a free parameter in the fitting procedure. We found that the difference of the best fit column density and the above fiducial value is less than several percent. Therefore, in order to keep the procedure simple and minimise the number of free parameters, we adopt the value $N_H = 7.23 \times 10^{22}$ from the paper of Zoglauer et al. (2015).

The results of our fit of the NuSTAR and Chandra spectral points using the model “power-law with exponential cutoff” in the general form of Eq.(1), i.e. leaving β , Γ and ϵ as free parameters, are shown in Table 1. One can see that the best fit gives a rather narrow range of the index β around 1/2. In Table we show separately also the results of the fits with three fixed values of β : 0, 1/2, and 1. While the pure-power law spectrum ($\beta = 0$) can be unambiguously excluded, the model of power-law with a simple exponential cutoff ($\beta = 1$) is not favourable either. It is excluded at the 3σ statistical significance level. In summary, the combined Chandra and NuSTAR data are best described by the index $\beta_e \approx 0.5$ and $\epsilon_0 \approx 1.5$ keV.

Whereas $\beta = 1/2$ seems to be a natural outcome (see below), the cutoff energy around 1.5 keV is a rather unexpected result. Namely, it implies that the acceleration of electrons in G1.9+0.3 proceeds significantly slower than one would anticipate given the very large, 14,000 km/s shock speed. This can be seen from the comparison of of the SED of G1.9+0.3 with one of the most effective particle accelerators in our Galaxy, ≈ 1600 year old SNR RX J1713.4-3946 (see Fig.2). The cutoff energy in the synchrotron spectrum of shock-accelerated electrons is proportional to the square of shock speed v_{sh}^2 (Aharonian & Atoyan 1999). Therefore, in order to exclude the difference in the cutoff energies caused by the difference in the shock speeds, we rescale the energies of the spectral points of RX J1713.4-3946 by the factor $(v_{sh}/14,000 \text{ km/s})^2$, where the shock speed of RX J1713.4-3946 is about $v_{sh} \approx 4,000$ km/s (Uchiyama et al. 2007). After such normalisation, the cutoff energy of RX J1713.4-3946 becomes an order of magnitude higher than the cutoff in G1.9+0.3. The acceleration of electrons in RX J1713.4-3946 proceeds close to the Bohm diffusion limit thus provides an acceleration rate close to the maximum value (Uchiyama et al. 2007; Zirakashvili & Aharonian 2010). Consequently, we may conclude that the current acceleration rate of electrons in G1.9+0.3 is lower, by an order of magnitude, compared to the maximum possible rate.

It should be noted that the physical meaning of Eq.(1) should not be overestimated. Namely, it should be considered as a convenient analytical presentation of the given set of measured spectral points. Consequently, the Γ , β , ϵ_0 that enter into Eq.(1), should be treated as a combination of formal fit parameters rather than physical quantities. For example, ϵ_0 in the exponential term of Eq.(1) should not necessarily coincide with the cutoff energy (or maximum in the SED). Indeed, in different $(\Gamma, \beta, \epsilon_0)$ combinations describing the same spectral points, the parameter ϵ_0 could have significantly different values. Analogously, Γ should not be

treated as a power-law index but rather a parameter which, in combination with Γ and β , determines the slope (the tangential) of the spectrum immediately before the cutoff region.

The maximum acceleration rate of particles is achieved when it proceeds in the Bohm diffusion limit. In the energy-loss dominated regime, the spectra of synchrotron radiation can be expressed by simple analytical formulae (Zirakashvili & Aharonian 2007). Because of compression of the magnetic field, the overall synchrotron flux of the remnant is dominated by the radiation from the downstream region (see Fig.3). The SED of the latter can be presented in the following form (Zirakashvili & Aharonian 2007)

$$\epsilon^2 \frac{dN}{d\epsilon} \propto \epsilon^2 (\epsilon/\epsilon_0)^{-1} [1 + 0.38(\epsilon/\epsilon_0)^{0.5}]^{11/4} \exp[-(\epsilon/\epsilon_0)^{1/2}]. \quad (2)$$

with

$$\epsilon_0 = \hbar\omega_0 = \frac{2.2 \text{ keV}}{\eta(1 + \kappa^{1/2})^2} \left(\frac{u_1}{3000 \text{ km s}^{-1}} \right)^2, \quad (3)$$

where η takes into account the deviation of the diffusion coefficient from its minimum value (in the nominal Bohm diffusion limit $\eta = 1$). In the standard shock acceleration theory, the momentum index of accelerated electrons $\gamma_s = 4$, and the ratio of the upstream and downstream magnetic fields, $\kappa = 1/\sqrt{11}$.

In Fig.3 the spectral points of G1.9+0.3 are compared with the theoretical predictions for synchrotron radiation in the upstream and downstream regions (Zirakashvili & Aharonian 2007). The calculations are performed for two values of the parameter η characterising the acceleration efficiency: $\eta = 1$ (Bohm diffusion regime) and 20 times slower ($\eta = 20$). The good (better than 20 %) agreement of the spectral points with the theoretical curves for $\eta = 20$ tells us that in G1.9+0.3 electrons are accelerated only at the 5 % efficiency level.

Although in the paper of Zoglauer et al. (2015) the spectral points are not explicitly presented, thus the direct comparison with our results is not possible, the conclusions of our study on the energy spectrum of G1.9+0.3 seems to be in agreement with the results of Zoglauer et al. (2015). However, because of the incorrect interpretation of the process of formation of the spectrum of synchrotron radiation, the statements in the paper by Zoglauer et al. (2015) are misleading (see Appendix A).

3. Relativistic electrons and magnetic fields

The joint treatment of X-ray and γ -ray data, under the simplified assumption that the same electron population is responsible for the broad-band radiation through the synchrotron and inverse Compton channels, provides information about the magnetic field and the total energy budget in relativistic electrons. G1.9+0.3 has been observed in VHE γ -ray band with the H.E.S.S. Cherenkov telescope system. Although no positive signal has been detected (H.E.S.S. Collaboration et al. 2014), the γ -ray flux upper limits allow meaningful constraints on the the average magnetic field in the X-ray and γ -ray production region. For calculations of the broad-band SED, we adopt the same background radiation fields used in the paper H.E.S.S. Collaboration et al. (2014): the infrared component with temperature of 48 K and energy density of 1.5 eVcm^{-3} , and the optical component with temperature of 4300 K and the energy density of 14.6 eVcm^{-3} . The comparison of model calculations with observations (see Fig.4) give a lower limit of the magnetic field, $B \geq 17 \mu\text{G}$.

Under certain assumptions, the magnetic field can be constrained also based only on the X-ray data. In the ‘‘standard’’ shock acceleration scenario, electrons are accelerated with the power-law index $\alpha = 2$. However because of the short radiative cooling time, their spectrum of highest energy electrons (the X-ray producers) becomes steeper, $\alpha = 2 \rightarrow 3$. Consequently, in the downstream region, where the bulk of synchrotron radiation is produced, X-rays have a photon index $\Gamma = 2$. The synchrotron cooling time can be expressed through the magnetic field and the X-ray photon energy: $t_{\text{synch}} \simeq 50(B/100\mu\text{G})^{-3/2}(\epsilon/1 \text{ keV})^{-1/2}$ years. Thus for $\epsilon \sim 1 \text{ keV}$ and the age of the SNR $\sim 150 \text{ yr}$, we find that the magnetic field should be larger than $50\mu\text{G}$.

The combined Chandra and NuSTAR data cover two decades in energy, from sub-keV to tens of keV. This allows derivation of the energy distribution of electrons, $W(E) = E^2 dN_e/dE$ in the most interesting region around the cutoff. The results shown in Fig.5 are obtained using the Markov Chain Monte Carlo (MCMC) code *Naima* developed by V. Zabalza¹. It is assumed that the magnetic field is homogeneous both in space and time. The results shown in in Fig.5 are calculated for the fiducial value of the magnetic field $B = 100 \mu\text{G}$, however they can be rescaled for any other value of the field. Note that while the shape of the spectrum does not depend on the strength of the magnetic field, the energies of individual electrons scale as $E \propto B^{-1/2}$, and the total energy contained in electrons scales as $\propto B^{-2}$. Since in the ‘‘standard’’ diffusive shock acceleration scenario the synchrotron X-ray flux is contributed mainly by the downstream region, the results in Fig.5 correspond to the range of the energy distribution of electrons for the same region. For comparison we show the energy distribution of electron calculated using the formalism of Zirakashvili & Aharonian (2007). Apparently, the good agreement between the derived electron spectrum with the theoretical curve for η naturally reflects the agreement between the X-ray observations and the theoretical predictions as demonstrated in Fig.3.

4. Conclusions

SNRs are believed to be the major contributors to the Galactic CRs. The recent detections of TeV emission from more than ten young SNRs (of the age of a few thousand years or younger), demonstrates the ability of these objects to accelerate particles, electrons and/or protons, to energies up to 100 TeV. Yet, we do not have observational evidence of extension of hard γ -ray spectra well beyond 10 TeV. Therefore one cannot claim an acceleration of protons and nuclei by SNRs to PeV energies. On the other hand, one cannot claim the opposite either, given the possibility that the acceleration of PeV protons and nuclei could happen at the early stages of evolution of SNRs when the shock speeds exceed 10,000 km/s. Then, the escape of the highest energy particles at later stages of evolution of SNRs can explain the spectral steepening of gamma-rays at multi-TeV energies from ≥ 1 thousand years old remnants.

In this regard, the youngest known SNR in our Galaxy, G1.9+0.3, with the measured shock speed 14,000 km/s, seems to be a unique object in our Galaxy to explorer the potential of SNRs for acceleration of protons and nuclei to PeV energies. Such measurements have been performed with the H.E.S.S. array of Cherenkov telescopes. Unfortunately, no positive signal has been detected. On the other hand, the recent observations

¹ <https://github.com/zblz/naima>

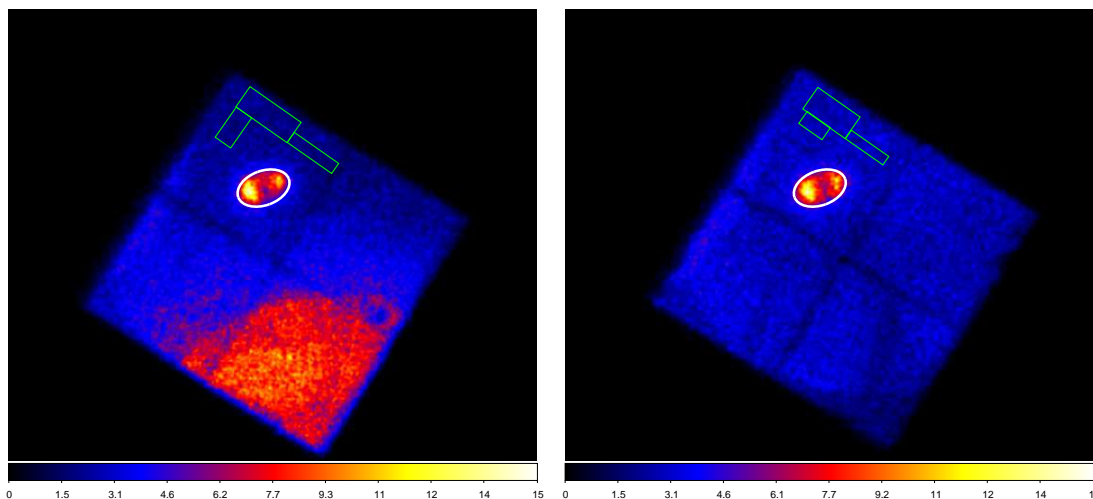


Fig. 1: Images from the observation 40001015007 for the FPMA (left) and FPMB (right) modules. The source and background regions are indicated by the white and green contours, respectively.

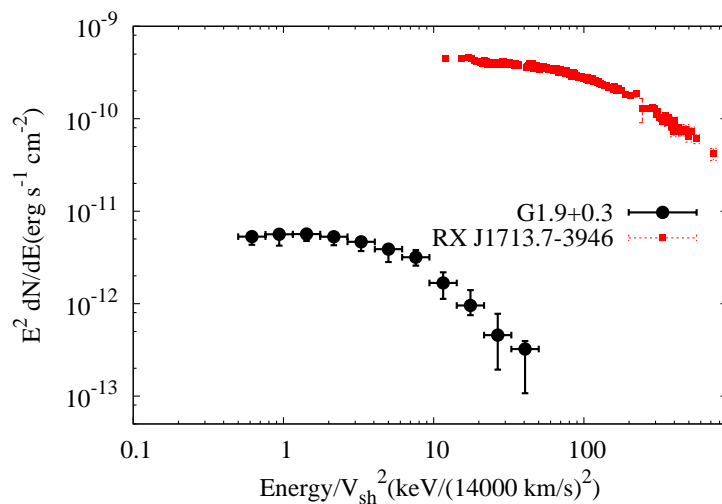


Fig. 2: The spectral points of G1.9+0.3 (this work; black circles) and RX J1713.4-3946 (red square) from Tanaka et al. (2008). The energies of the points of RX J1713.4-3946 are rescaled by the factor of the square of the ratio of shock speeds of J1713.4-3946 and G1.9+0.3: $(14,000 \text{ km/s}/4000 \text{ km/s})^2 = 12.25$.

Table 1: Spectral Fitting results for G1.9+0.3

model	PL index	cutoff (keV)	β	$\chi^2/d.o.f.$
PL	2.54 (2.52 - 2.56)			1089.4/666
PL+ecut	2.04 (1.98 - 2.10)	11.8 (10.5 - 13.3)		697.7/665
PL+ecut ($\beta=0.5$)	1.65 (1.60 - 1.70)	1.68 (1.50 - 1.90)	0.5	686.2/665
PL+ecut (β free)	1.62(1.48 - 1.75)	1.41 (1.30-1.55)	0.48 (0.40-0.56)	685.8/664

of G1.9+0.3 in hard X-rays by NuSTAR provide unique information about the acceleration efficiency of electrons. Together with Chandra data at lower energies, these data allow model-independent conclusions. Although the general shape of the energy spectrum of X-rays is in a very good agreement with predictions of the diffusive shock-acceleration theory, the acceleration rate appears an order of magnitude slower relative to the maximum acceleration rate achieved in the nominal Bohm diffusion limit. To a certain extent, this is a surprise, especially when compared with young SNRs like Cas A and RX J1713.4-3946 in

which the acceleration of electrons proceeds in the regime close to the Bohm diffusion. If the acceleration of protons and nuclei proceeds in the same manner as the electron acceleration, this result could have a negative impact on the ability of G1.9+0.3 to operate as a PeVatron. Apparently, the observations of G1.9+0.3 alone are not sufficient to conclude whether this conclusion can be generalised for other SNRs.

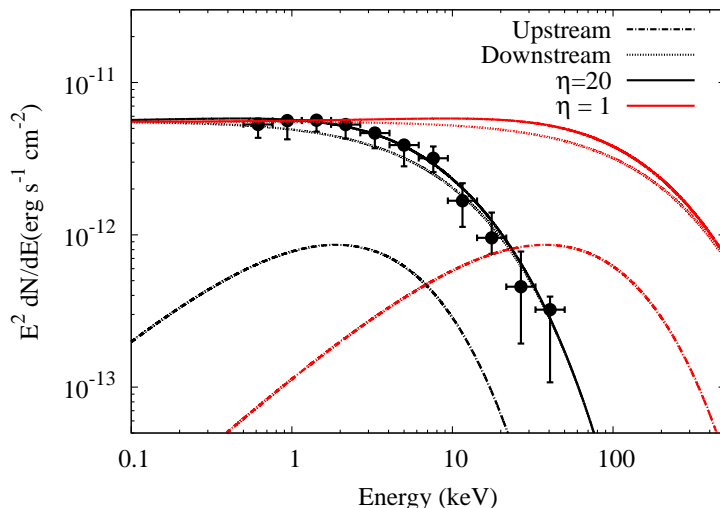


Fig. 3: The spectral points of G1.9+0.3 (this work) compared to the predictions of synchrotron radiation of the shock accelerated electrons in the downstream and upstream regions (Zirakashvili & Aharonian 2007) for two regimes of diffusion: Bohm diffusion $\eta = 1$ and 20 times faster, $\eta = 20$.

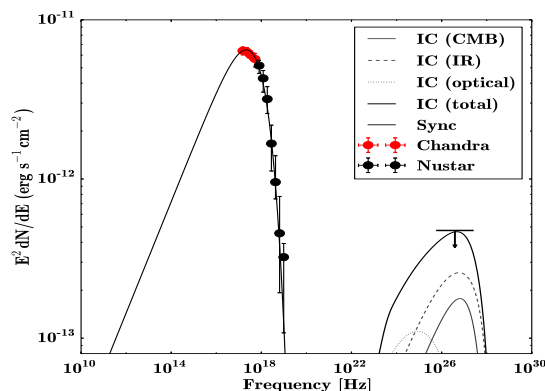


Fig. 4: X-ray SED as well as the VHE upper limit from H.E.S.S. Collaboration et al. (2014). The curves are the synchrotron and IC emissions fitted to derive the lower limit of the magnetic field.

Appendix A:

The cutoff region in the distribution of parent electrons $F(E)$ has a shape similar to the synchrotron spectrum given by Eq.(2), $F(E) \propto \exp[-(E/E_0)^\beta]$ with the following simple relation between β_e and β (Fritz 1989):

$$\beta = \frac{\beta_e}{2 + \beta_e}. \quad (\text{A.1})$$

Thus the cutoff region in the spectrum of synchrotron radiation is much smoother than the cutoff region in of the spectrum of parent electrons. For any electron distribution, the the synchrotron cutoff cannot be sharper than the simple exponential decline ($\beta = 1$) which can be realised only in the case of an abrupt cutoff in the spectrum of parent electrons ($\beta_e \rightarrow \infty$). In the case of a simple exponential cutoff in the electron spectrum ($\beta_e = 1$), the corresponding synchrotron cutoff region is very shallow with $\beta = 1/3$. Formally, such spectra can be formed during the shock acceleration of electrons in the Bohm diffusion regime when the maximum energy of electrons is determined by the age of the source rather than by energy losses of electrons.

However, in the particular case of young SNRs when the electrons are accelerated up to 100 TeV and beyond (otherwise one cannot explain the observed X-ray data), any reasonable set of parameters (magnetic field, age of the source, shock speed, *etc.*), the acceleration proceeds in the electron energy-loss regime, and the maximum energy is determined from the competition between the acceleration and energy loss rates. In this case, the spectrum of electrons exhibits a super exponential cutoff, namely $\beta_e = 2$ (Zirakashvili & Aharonian 2007). Correspondingly, the synchrotron spectrum contains, in accordance with Eq.(3), a cutoff with $\beta = 1/2$.

The δ -functional approximation gives wrong relation between β_e and β , namely $\beta = \beta_e/2$. For example, within this approximation, the cutoff in the spectrum of synchrotron radiation with $\beta = 1$ can be interpreted as a result of the cutoff in the electron spectrum with $\beta_e = 2$. However, in reality, such a synchrotron spectrum can be formed, in accordance with Eq.(2), in the case of an abrupt cutoff in the electron spectrum, i.e. $\beta_e \rightarrow \infty$. Another remark regarding the srcut model. The cutoff in the synchrotron spectrum with $\beta = 1/2$ is formed by the highest energy electrons with $\beta_e = 2$ (see Eq.(2)) but not with $\beta_e = 1$, as it follows from the δ -functional approximation. Therefore the often

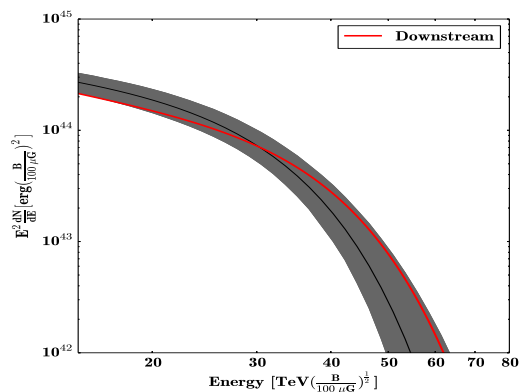


Fig. 5: Electron spectrum from the x-ray data points (black curve and shaded area) and theoretical predicted integrated electron spectrum in young SNR (red curve) assuming a fast diffusion, i.e., $\eta = 20$ in Eq.1. Also shown is the contribution from downstream region.

claims in the literature that the δ -functional approximation gives correct synchrotron spectrum (see, e.g., Reynolds 2008) is not only wrong, but leads to misleading conclusions. For example, while the fit of the X-ray data by a *script* type spectrum is a clear indication of acceleration of electrons in the energy-loss regime, the same result has been interpreted by (Zoglauer et al. 2015) as acceleration in the regime free of energy losses.

References

- Aharonian, F. A. 2013, *Astroparticle Physics*, 43, 71
 Aharonian, F. A. & Atoyan, A. M. 1999, *A&A*, 351, 330
 Bamba, A., Fukazawa, Y., Hiraga, J. S., et al. 2008, *PASJ*, 60, S153
 Blasi, P. 2013, *A&A Rev.*, 21, 70
 Fritz, K. D. 1989, *A&A*, 214, 14
 Green, D. A., Reynolds, S. P., Borkowski, K. J., et al. 2008, *MNRAS*, 387, L54
 H.E.S.S. Collaboration, Abramowski, A., Aharonian, F., et al. 2014, *MNRAS*, 441, 790
 Hillas, A. M. 2013, *Astroparticle Physics*, 43, 19
 Malkov, M. A. & Drury, L. O. 2001, *Reports on Progress in Physics*, 64, 429
 Reynolds, S. P. 2008, *ARA&A*, 46, 89
 Reynolds, S. P., Borkowski, K. J., Green, D. A., et al. 2008, *ApJ*, 680, L41
 Reynolds, S. P., Borkowski, K. J., Green, D. A., et al. 2009, *ApJ*, 695, L149
 Stage, M. D., Allen, G. E., Houck, J. C., & Davis, J. E. 2006, *Nature Physics*, 2, 614
 Tanaka, T., Uchiyama, Y., Aharonian, F. A., et al. 2008, *ApJ*, 685, 988
 Uchiyama, Y., Aharonian, F. A., Tanaka, T., Takahashi, T., & Maeda, Y. 2007, *Nature*, 449, 576
 Wik, D. R., Hornstrup, A., Molendi, S., et al. 2014, *ApJ*, 792, 48
 Zirakashvili, V. N. & Aharonian, F. 2007, *A&A*, 465, 695
 Zirakashvili, V. N. & Aharonian, F. A. 2010, *ApJ*, 708, 965
 Zoglauer, A., Reynolds, S. P., An, H., et al. 2015, *ApJ*, 798, 98